# Data-informed uncertainty quantification for wave scattering by heterogenous media

M. Ganesh[1] S. C. Hawkins[2] N. Kordzakhia[3]
L. Stals[4]

(Received 31 January 2023; revised 16 November 2023)

**Abstract**

We present an efficient data-driven offline/online Bayesian algorithm for uncertainty quantification (UQ) in the induced scattered field when a time-harmonic incident wave interacts with an uncertain heterogeneous medium. The incident wave of interest need not be known in advance, and the uncertainty is informed by noisy scattering data obtained from other incident waves impinging on the medium. Our UQ algorithm is accelerated by a novel stochastic reduced order model (ROM) based on the T-matrix, and the ROM is independent of both the incident wave, and other incident waves used to generate the data. This important property allows the model to be set up offline.

DOI:10.21914/anziamj.v64.17965,  Published 2023-11-27, as part of the Proceedings of the 20th Biennial Computational Techniques and Applications Conference. ISSN 1445-8810. (Print two pages per sheet of paper.) 

# Contents

1 Introduction C100

2 A stochastic T-matrix reduced order model C103

3 Uncertainty quantification of wave model C107

4 Numerical results C109

# 1 Introduction

We consider the interaction of time harmonic incident waves $u^{inc}$ with a heterogeneous medium occupying a bounded region $D \subseteq \mathbb{R}^2$, with real refractive index $n$. The non-absorbing medium, with $n(x) = \sqrt{1 - m(x)}$ for $x \in \overline{D}$, is characterised by its contrast function $m$ with support contained in $D$ (ensuring that the refractive index in the exterior free-space $D^c := \mathbb{R}^2 \setminus \overline{D}$ is constant). Here, $\overline{D} = D \cup \partial D$, with $\partial D$ being the boundary of the domain $D$. Interaction of the incident wave (from $D^c$) with the medium induces a scattered wave $u^s$ such that the total wave $u = u^{inc} + u^s$ satisfies the Helmholtz equation

$$\Delta u(x) + k^2(1 - m)u(x) = 0, \quad x \in \mathbb{R}^2. \tag{1}$$

Here $k = 2\pi/\lambda$ is the wavenumber in the unbounded region $D^c$, and $\lambda$ the incident wavelength. The scattered field $u^s$ is also required to satisfy the Sommerfeld radiation condition [5, eq. (3.108)].

We focus on uncertainty quantification for the far field of $u^s$ when the contrast function $m$ is uncertain, conditioned on the far field data obtained for certain incident and observation directions. The far field of interest is induced by an incident plane wave with direction different, in general, to the incident waves for which the data is obtained. The far field $u^\infty$ is defined in relation to the

scattered wave as

$$u^s(x) = \frac{e^{ikr}}{\sqrt{r}} \left[ u^\infty(\hat{x}) + O(1/r) \right], \tag{2}$$

where $r = |x|$. The limit holds uniformly with respect to the observation direction $\hat{x} = x/r \in \partial B$, where $\partial B \subseteq \mathbb{R}^2$ denotes the set of all directions.

In Figure 1 we illustrate a model configuration that has an incident wave impinging on the medium with direction $d_0$ associated with the data, and a second incident wave with direction $d^*$ associated with the quantity of interest. Such configurations are simple models for medical applications in which ultrasound is focused, and the focusing takes account of the low-contrast heterogeneity of the body tissue through which the ultrasound propagates [16], which must be inferred through data.

The uncertainty quantification problem in this work is closely related to the inverse medium problem, and we refer to the most recent edition of the book by Colton and Kress for the state of the art in this subject [5]. Typically the forward problem (1) is solved using coupled FEM-BEM algorithms [14], the Lippmann–Schwinger equation [13] or the Born approximation [2, 4]. The Born approximation [5, Section 8.4]

$$v^\infty(\hat{x}; m) = -k^2 \int_D G^\infty(\hat{x}, y)\, m(y)\, u^{inc}(y)\, dy, \quad \hat{x} \in \partial B, \tag{3}$$

gives an approximation to the far field $u^\infty$ that is valid when the contrast $c = \sup_{x \in D} |m(x)|$ is small, or for low wavenumber. Here

$$G^\infty(\hat{x}, y) = \frac{1+i}{4\sqrt{\pi k}} e^{-ik\hat{x}\cdot y}, \tag{4}$$

is derived from the free-space Green's function of the Helmholtz equation, and $v^\infty(\cdot; m)$ in (3) explicitly indicates dependence of the far field on $m$. In this work, we assume that the low-contrast medium satisfies $(ka)^2 c \ll 2$, where $a$ denotes the radius of $D$, so that the Born approximation (3) is valid and approximation results of Colton and Kress [5, Section 8.2] can be applied. The

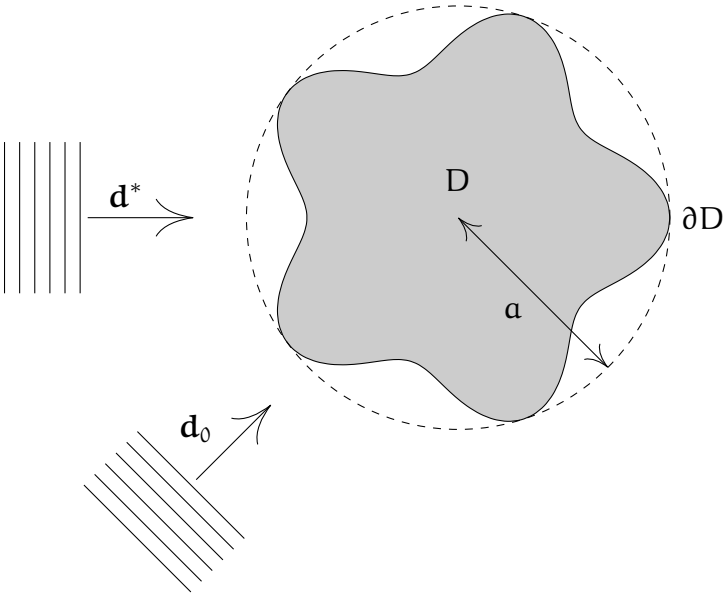


Figure 1: Schematic showing a heterogeneous medium occupying D, with boundary $\partial$D, illuminated by an incident wave with direction $\mathbf{d}_0$ (associated with the far field data) and an incident wave with direction $\mathbf{d}^*$ (associated with the quantity of interest).

Born approximation is considered to be sufficient for several inverse problem applications [5], including flaw characterization using ultrasound [18]. In the next section we describe an efficient method to use $\mathfrak{v}^\infty(\cdot\,;\mathfrak{m})$ to efficiently construct an approximation to $\mathfrak{u}^\infty(\widehat{\mathbf{x}})$ for any observation direction $\widehat{\mathbf{x}}$.

The key idea in this work is to use a stochastic counterpart of the T-matrix [8] to facilitate computing the uncertain far field from the Born approximation without knowing the incident and observation directions in advance. In Section 2 we describe a T-matrix-based ROM for computing the far field. In Section 3 we use the T-matrix for efficiently sampling the data-informed posterior distribution for the far field of interest. In Section 4 we demonstrate our algorithm by performing uncertainty quantification for a challenging test

problem with a piecewise constant heterogeneous medium.

## 2 A stochastic T-matrix reduced order model

For simplicity, we let our quantity of interest be the far field $u^\infty(\widehat{\mathbf{x}})$ induced by the incident wave $u^{\text{inc}}(\mathbf{x}) = e^{\mathrm{i}k\mathbf{x}\cdot\mathbf{d}^*}$ with arbitrarily chosen, but known, direction $\mathbf{d}^*$. Our uncertainty quantification algorithm for $u^\infty(\widehat{\mathbf{x}})$ has two parts. The first part involves offline construction of a reduced order model based on deterministic T-matrices associated with an ansatz of the contrast function. The key here is that such T-matrices can be constructed offline. The second part involves fast online uncertainty quantification for $u^\infty(\widehat{\mathbf{x}})$, through uncertain coefficients of the ansatz and associated stochastic T-matrix. The observation directions $\widehat{\mathbf{x}}$ and the incident wave direction $\mathbf{d}^*$ are not required for the first part of the algorithm, and once constructed offline, the reduced order model can be used for any $\widehat{\mathbf{x}}$ and $\mathbf{d}^*$.

The deterministic T-matrix derivation is based on the idea that for a fixed and known refractive index, the wave model is governed by the *linear* Helmholtz operator transforming an input incident wave into an associated radiating scattered field. Through series expansions of the incident and scattered fields using classical regular wave functions (involving the Bessel functions) and radiating wave functions (involving the Hankel functions), respectively, the model is equivalently considered to be governed by an infinite T-matrix transforming the infinite number of coefficients in the incident wave expansion into those in the scattered field expansion. The far field series expansion of the wave model is obtained by taking the far field of the radiating wave functions (that are stable complex exponentials) and hence the T-matrix can also be considered as an operator transforming the incident field expansion coefficients into those of the far field. For a stable construction of the T-matrix and key properties, including the configuration shape independent convergence of the truncated-expansions-based T-matrix, we refer to Ganesh, Hawkins and Hiptmair [9], Ganesh and Hawkins [7] and references therein.

Our offline algorithm is based on the regular wavefunction expansion of the incident wave as

$$u^{\mathrm{inc}}(\boldsymbol{x}) = \sum_{\ell=-\infty}^{\infty} b_\ell J_{|\ell|}(kr) e^{i\ell\theta}, \tag{5}$$

where we use polar coordinates $\boldsymbol{x} = (r\cos\theta, r\sin\theta)$ with origin $\mathbf{0}$, and we assume that $\mathbf{0} \in D$. Here $J_\ell$ is the Bessel function of order $\ell$. For incident plane waves $u^{\mathrm{inc}}(\boldsymbol{x}) = e^{ik\boldsymbol{x}\cdot\boldsymbol{d}}$, with wave direction $\boldsymbol{d} = (\cos\phi, \sin\phi)$, the input expansion coefficients are known analytically [5, Equation (3.112)],

$$b_\ell = i^{|\ell|} e^{-i\ell\phi}. \tag{6}$$

The corresponding expansion, with unknown coefficients, of the far field is

$$u^\infty(\widehat{\boldsymbol{x}}) = \sum_{\ell=-\infty}^{\infty} a_\ell \sqrt{\frac{1}{\pi k}} (-i)^{|\ell|} (1-i) e^{i\ell\theta}, \tag{7}$$

and the vector of expansion coefficients $(a_\ell)$ is obtained from the vector of incident wave coefficients $(b_\ell)$ by

$$(a_\ell) = T(b_\ell), \tag{8}$$

where $T = [t_{\ell'\ell}]$ is the T-matrix of the scatterer [8]. The entries in the T-matrix are given by Ganesh and Hawkins [6, 8] as

$$t_{\ell'\ell} = \frac{1}{4}\sqrt{\frac{k}{\pi}} i^{|\ell'|} (1+i) \int_0^{2\pi} v_\ell^\infty(\widehat{\boldsymbol{x}}; m)\, e^{-i\ell'\theta}\, d\theta, \tag{9}$$

where $\widehat{\boldsymbol{x}} = (\cos\theta, \sin\theta)$. Here we use the Born approximation

$$v_\ell^\infty(\widehat{\boldsymbol{x}}; m) = -k^2 \int_D G^\infty(\widehat{\boldsymbol{x}}, \boldsymbol{y})\, m(\boldsymbol{y})\, u_\ell^{\mathrm{inc}}(\boldsymbol{y})\, d\boldsymbol{y}, \quad \widehat{\boldsymbol{x}} \in \partial B, \tag{10}$$

to compute the far field induced by the incident wave $u_\ell^{\mathrm{inc}}(\boldsymbol{y}) = J_{|\ell|}(k\rho) e^{i\ell\phi}$, and make use of polar coordinates $\boldsymbol{y} = (\rho\cos\phi, \rho\sin\phi)$.

We introduce an ansatz for the uncertain contrast function

$$\mathfrak{m}(\mathbf{y}) = \sum_{j=1}^{M} \mu_j \mathfrak{m}_j(\mathbf{y}), \quad \mathbf{y} \in D, \tag{11}$$

where the coefficients $\mu_j$ are uncertain, and $\mathfrak{m}_j$ for $j = 1, \ldots, M$ are appropriate deterministic basis functions. Our motivation for the above ansatz is that through the Spectral Theorem applied for a compact normal Hilbert–Schmidt (H-S) integral operator on $L^2(D)$, the classical Kosambi–Karhunen–Loève (KKL, but widely abbreviated as KL) theorem provides a robust theoretical foundation for a series expansion of a stochastic process (such as $\mathfrak{m}$) using a class of orthogonal basis functions that are eigenfunctions of the H-S integral operator, with associated H-S kernel (defined on $D \times D$) corresponding to the covariance of the stochastic process. In practice, the KKL expansion needs to be truncated, leading to an approximate KKL ansatz with appropriate basis functions [e.g. 10, and references therein] in which *localized* KKL eigenfunctions with sub-domain covariances are used for a stochastic model with epistemic uncertainties.

Except for the case of simple geometries $D$ (typically with harmonics as eigenfunctions), finding the KKL eigenfunction solutions of the H-S kernel-based second-kind Fredholm integral equation (FIE or equivalent PDE) requires numerical approximations of the FIE/PDE in finite dimensional subspaces of $L^2(D)$ [10]. Finite dimensional subspaces spanned by splines or radial basis functions (such as thin plate splines) have been widely used to approximately solve FIEs and PDEs. Thus, in general, a practical truncated KKL-type ansatz is spanned by basis functions used in standard numerical methods for FIE/PDE. Even for the case of simple geometries for which analytical global harmonic eigenfunctions are known, use of localized basis functions in KKL-type expansions for representing uncertain random fields may be preferred. For example, Bachmayr and Djurdjevac [1, and references therein] show the advantages of using a non-standard KKL-type basis ansatz even for the simple sphere geometry.

Our goal is to develop an approach that can be applied to complex domains

and in this article we use a mixed finite element approximation to thin plate splines (TPS) [17] as basis functions in the ansatz (11). Quantifying the uncertain coefficients (as random variables) is data-driven through an offline/online Bayesian framework, and we avoid solving the KKL eigenvalue problem. For a PDE-based proof on the TPS interpolation approximation properties with improved error estimates, we refer to Lohndorf and Melenk [15, and references therein].

In this article, evaluation of the TPS is restricted to $D$, and the main challenge is to choose the control points. We use the nodes of a coarse triangular mesh tessellation of $D$, noting that such tessellations can be computed easily even for complex domains. Using the linearity of (9)–(10) with respect to $\mathfrak{m}$, we write the model-associated stochastic T-matrix as

$$T = \sum_{j=1}^{M} \mu_j T^{(j)}, \tag{12}$$

where $T^{(j)} = [t^{(j)}_{\ell'\ell}]$ is the deterministic T-matrix associated with the known basis functions $\mathfrak{m}_j$ for $j = 1, \dots, M$, where

$$t^{(j)}_{\ell'\ell} = \frac{1}{4}\sqrt{\frac{k}{\pi}} i^{|\ell'|}(1+i) \int_0^{2\pi} v^{\infty}_{\ell}(\widehat{x}; \mathfrak{m}_j)\, e^{-i\ell'\theta}\, d\theta\,. \tag{13}$$

In general, the T-matrix is not linear with respect to the contrast function, but linearity of $T$ as a function of the basis functions holds here because the Born approximation used to compute the T-matrix entries in (10)–(13) is linear in $\mathfrak{m}$, and hence $T$ is linear in $\mathfrak{m}$ as well.

In practice the series (5)–(7) and the T-matrix are truncated for $-N \leqslant \ell, \ell' \leqslant N$ where $N$ is a truncation parameter. In this work we compute $N$ based on the wavenumber using Wiscombe's formula [19]. Based on the truncation parameter $N$, the integral in (13) is approximated to high accuracy using the $2N+2$ point rectangle rule

$$\int_0^{2\pi} v^{\infty}_{\ell}(\widehat{x}; \mathfrak{m}_j) e^{-i\ell'\theta}\, d\theta \approx \sum_{i=0}^{2N+1} \nu_i v^{\infty}_{\ell}((\cos\theta_i, \sin\theta_i); \mathfrak{m}_j) e^{-i\ell'\theta_i}, \tag{14}$$

where the rectangle points are $\theta_i = 2\pi i/(2N+2)$ and the weights are $\nu_i = \pi/(N+1)$. Thus the T-matrices $T^{(j)}$ are computed using far-field data from the fixed observation angles $\theta_i$ for $i = 0, \ldots, 2N+1$, but they can then be used to efficiently compute the far field for any observation angle $\theta$, and indeed for any incident wave direction $\mathbf{d}^*$.

# 3 Uncertainty quantification of wave model

We model the parameters $\mu_j$ in (11) and (12), for $j = 1, \ldots, M$, as random variables in a probability space $\Omega$. Using Bayes' Theorem, the posterior probability distribution for $\boldsymbol{\mu} = (\mu_j)$, informed by far field data $\mathbf{f}$, satisfies

$$p(\boldsymbol{\mu}, \sigma \mid \mathbf{f}) \propto p(\mathbf{f} \mid \boldsymbol{\mu}, \sigma)\, p(\boldsymbol{\mu})\, p(\sigma)\,, \tag{15}$$

where $p(\boldsymbol{\mu})$ is the prior distribution for $\boldsymbol{\mu}$, which encapsulates any a-priori knowledge or assumptions about the contrast function $\mathfrak{m}$, and $p(\sigma)$ is the prior distribution for the noise $\sigma$. We assume that the $\mu_j$ for $j = 1, \ldots, M$ are independent with Gaussian distributions having zero mean and variance $\omega^2$, so that

$$p(\boldsymbol{\mu}) = \frac{1}{(2\pi\omega^2)^{M/2}} \exp\left(-\frac{\|\boldsymbol{\mu}\|_2^2}{2\omega^2}\right). \tag{16}$$

The contrast function $\mathfrak{m}$ is real because the medium is non-absorbing. It is convenient to enforce real coefficients $\boldsymbol{\mu}$ by using real-valued data obtained by splitting $n$-dimensional complex-valued far field data into real and imaginary components. Consequently, we assume the real valued data $\mathbf{f} \in \mathbb{R}^{2n}$ includes Gaussian noise in each component, having zero mean and variance $\sigma^2$. Then the likelihood function is

$$(\mathbf{f} \mid \boldsymbol{\mu}, \sigma) = \frac{1}{(2\pi\sigma^2)^n} \exp\left(-\frac{\|C\boldsymbol{\mu} - \mathbf{f}\|_2^2}{2\sigma^2}\right), \tag{17}$$

where the $2n \times M$ matrix $C = [c_{ij}]$ is

$$c_{2i-1,j} = \operatorname{Re} v^\infty(\widehat{\mathbf{x}}_i\,; \mathfrak{m}_j)\,, \quad c_{2i,j} = \operatorname{Im} v^\infty(\widehat{\mathbf{x}}_i\,; \mathfrak{m}_j)\,, \quad i = 1, \ldots, n\,. \tag{18}$$

Here $v^\infty(\cdot\,;\mathfrak{m}_j)$ is the far field induced by the incident wave $u^{\mathrm{inc}}(\mathbf{x}) = e^{\mathrm{i}k\mathbf{x}\cdot\mathbf{d}_0}$ and $\widehat{\mathbf{x}}_1, \ldots, \widehat{\mathbf{x}}_n \in \partial B$ are the observation directions for the data. The far field data $\mathbf{f}$ is constructed similarly. We sample $(\boldsymbol{\mu}, \sigma)$ from the posterior (15) using the Gibbs sampler [3] with a log-uniform distribution for $\sigma$. The samples of $\boldsymbol{\mu}$ are then samples of the marginal distribution (with $\sigma$ integrated out).

Although $v^\infty(\widehat{\mathbf{x}}_i\,;\mathfrak{m}_j)$ can be computed directly from (3) using numerical evaluation of the integral, it is more efficient to use the T-matrix in (12), which—in contrast to (3)—is independent of the observation directions and hence can be computed offline beforehand. In particular, using the T-matrix and the expansion (7) we have

$$c_{2i-1,j} + c_{2i,j}\mathrm{i} = \sum_{\ell=-N}^{N} \left(T^{(j)}(b_\ell)\right)_\ell \sqrt{\frac{1}{\pi k}}(-\mathrm{i})^{|\ell|}(1-\mathrm{i})e^{\mathrm{i}\ell\theta_i}\,. \tag{19}$$

In the numerical experiments in Section 4 we exploit that the T-matrix is also independent of the incident wave direction, which affects only the coefficients $(b_\ell)$ in (19). Thus data for incident waves with several different incident directions is incorporated efficiently.

The maximiser $\boldsymbol{\mu}_{\mathrm{MAP}}$ of the posterior distribution (15) minimises the functional

$$\|C\boldsymbol{\mu}_{\mathrm{MAP}} - \mathbf{f}\|_2^2 + \tau^2\|\boldsymbol{\mu}_{\mathrm{MAP}}\|_2^2\,, \tag{20}$$

where $\tau = \sigma/\omega$, and is computed as the solution of

$$\left(C^*C + \tau^2 I\right)\boldsymbol{\mu}_{\mathrm{MAP}} = C^*\mathbf{f}\,. \tag{21}$$

Then $\boldsymbol{\mu}_{\mathrm{MAP}}$ is used to compute the associated quantity of interest $v^\infty(\widehat{\mathbf{x}}\,;\boldsymbol{\mu})$ induced by the incident plane wave $u^{\mathrm{inc}}(\mathbf{x}) = e^{\mathrm{i}k\mathbf{x}\cdot\mathbf{d}^*}$. Here we write $v^\infty(\widehat{\mathbf{x}}\,;\boldsymbol{\mu})$ for $v^\infty(\widehat{\mathbf{x}}\,;\mathfrak{m})$ where $\mathfrak{m}$ is obtained from $\boldsymbol{\mu}$ using (11) and, using the T-matrix,

$$v^\infty(\widehat{\mathbf{x}}\,;\boldsymbol{\mu}) = \sum_{\ell=-N}^{N} a_\ell \sqrt{\frac{1}{\pi k}}(-\mathrm{i})^{|\ell|}(1-\mathrm{i})e^{\mathrm{i}\ell\theta}\,, \tag{22}$$

with equations (8) and (12), and where $(b_\ell)$ is the vector of expansion coefficients of $u^{\mathrm{inc}}$ given by (6).

Samples of (15) computed using the Gibbs sampler provide more information about the posterior distribution than $\mu_{\mathrm{MAP}}$ alone. The samples are used to compute statistical properties of the quantity of interest such as the mean

$$\mathbb{E}[v^\infty(\hat{x};\cdot)] \approx \frac{1}{m}\sum_{i=1}^{m} v^\infty(\theta;\mu_i)\,, \tag{23}$$

where $\mu_1,\ldots,\mu_m$ are samples from (15). Statistical properties of the contrast function $m$ given by (11) may also be of interest.

# 4 Numerical results

We demonstrate our algorithm in Matlab with noisy test data obtained by simulating scattering by three small penetrable homogeneous scatterers with contrast given by the function $m(x) = 10^{-2}$ for $x$ inside the scatterers and zero for $x$ exterior to the scatterers. The scatterers are inside the unit disk $D$ and the wavenumber is $k = 8$, so that the diameter of $D$ is about $2.5\lambda$ and the diameter of the scatterers is about $0.5\lambda$. The far field of the medium is computed to high accuracy using the MieSolver package [11], and Gaussian noise with standard deviation 1% is added to obtain the data, which is publicly available [12]. In MieSolver we apply transmission boundary conditions on the interfaces of the scatterers with continuity of the total field and its normal derivative. The contrast function is visualised in Figure 2(left).

We use the ansatz (11) for the data-informed approximation to the contrast function. The basis functions $m_j$ are thin plate splines constructed to approximately interpolate at 90 points on a coarse tessellation of $D$. The smoothness of the TPS, one of which is visualised in Figure 3, provides a smooth interpolant throughout $D$ with only a small number of control points, with error estimates given by Löhndorf and Melenk [15]. The splines corresponding to the 57 interior control points are used for the ansatz (11), and $m$

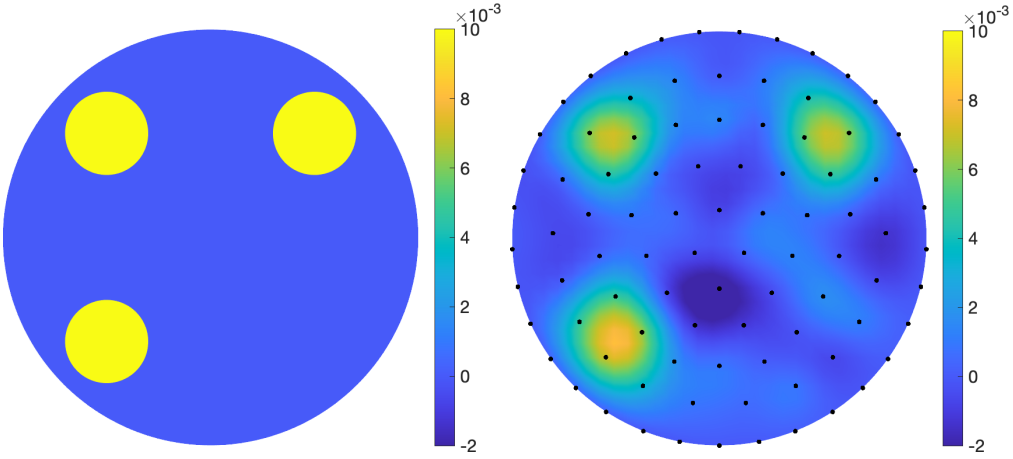


Figure 2: Visualisation of the target contrast function $\mathfrak{m}(\mathfrak{x})$ (left); and the expected value of the reconstruction (right) with the thin plate spline control points marked.

implicitly approximates zero at the boundary control points. The offline/online UQ algorithm in Section 3 is therefore undertaken over an $M = 57$ dimensional stochastic space. We sample the posterior distribution using the Gibbs sampler with $\omega = 5 \times 10^{-3}$ in the prior distribution (16).

The T-matrices $T^{(j)}$ in Section 2 are computed using the TMATROM package [8] and the Born approximation integrals in (10) are computed using quadrature rules defined on a triangular mesh tessellation of $D$. The integrands in the Born approximation are smooth because the thin plate spline basis functions $\mathfrak{m}_j$ are smooth. The test problem used here is challenging because the piecewise-constant target contrast function is discontinuous and our ansatz (11) is continous. However, the piecewise constant contrast function allows us to use the MieSolver algorithm, so that the solver we use to generate the data is completely independent of the solver we use for the UQ and there is no "inverse crime" [5, Page 179].

In Figure 4 we visualise the UQ performed using $s = 10\,000$ samples of

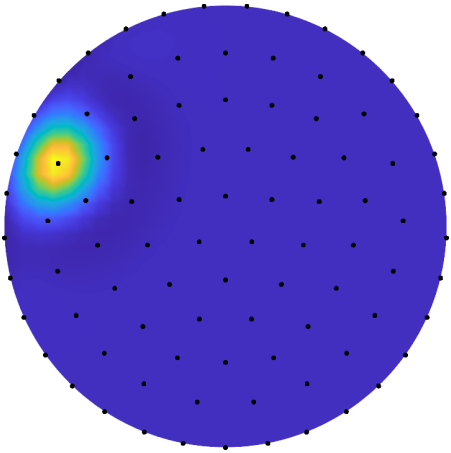

Figure 3: Visualisation of a typical thin plate spline $\mathfrak{m}_j$ with the control points marked.

the posterior distribution for an incident plane wave with direction $\mathbf{d}^* = (\cos\pi/6, \sin\pi/6)$ by plotting the expected value (23) and the two-sigma confidence region. The far field associated with the maximiser $\boldsymbol{\mu}_{\text{MAP}}$ of the posterior distribution is also shown. The figure shows excellent agreement between the predicted far field and the true value computed using MieSolver. The incident wave directions used to generate the data are indicated in the figure and highlight that incident wave direction $\mathbf{d}^*$ was not one of the these. In Figure 2(right) we visualise the expected value of the noisy data-driven uncertain contrast function computed using the same samples.

**Acknowledgements** This work was supported by EPSRC Grant Number EP/R014604/1, by grants from the Simons Foundation, and by an Australian Research Council grant (DP220102243). Dr. Hawkins thanks the Isaac Newton Institute for Mathematical Sciences for support and hospitality during the programme Mathematical Theory and Applications of Multiple Wave Scattering, when work on this manuscript was undertaken.

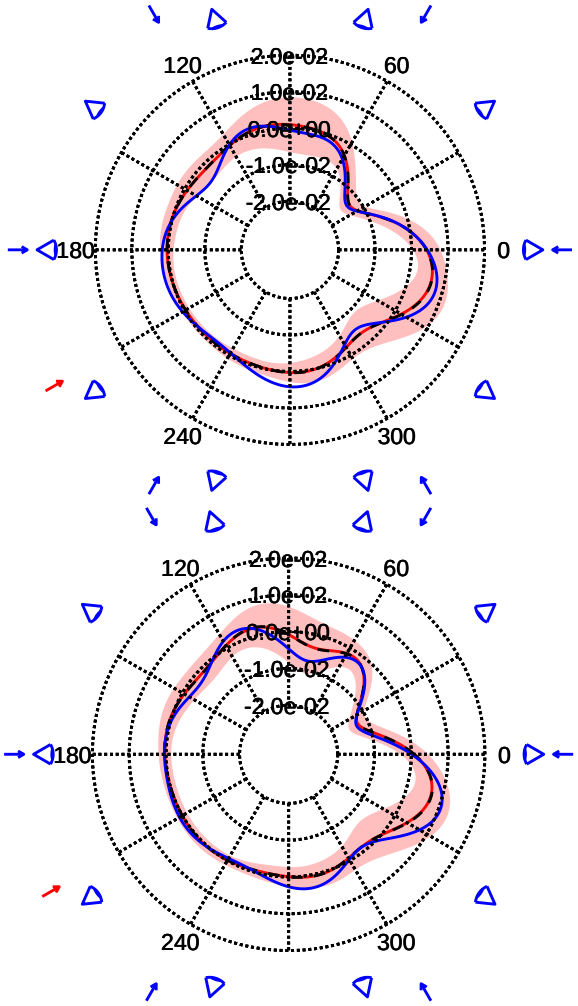


Figure 4: Uncertainty quantification for the real part (top); and imaginary part (bottom) of the far field induced by the uncertain medium. The expected value is shown in red, with plus/minus two standard deviations marked with red shading. The value associated with the maximum of the posterior distribution is shown in black (dashed line). The true far field is shown in blue. The incident wave and observation directions used for the data are indicated in blue. The incident wave direction used for uncertainty quantification is indicated in red.

# References


[1] M. Bachmayr and A. Djurdjevac. "Multilevel representations of isotropic Gaussian random fields on the sphere". In: *IMA J. Numer. Anal.* 43.4 (2023), pp. 1970–2000. DOI: 10.1093/imanum/drac034 (cit. on p. C105).

[2] C. Borges and G. Biros. "Reconstruction of a compactly supported sound profile in the presence of a random background medium". In: *Inv. Prob.* 34, 115007 (2018). DOI: 10.1088/1361-6420/aadbc5 (cit. on p. C101).

[3] G. Casella and E. I. George. "Explaining the Gibbs Sampler". In: *Am. Stat.* 46 (1992), pp. 167–174. DOI: 10.1080/00031305.1992.10475878 (cit. on p. C108).

[4] Y. Chen. In: *Inv. Prob.* 13 (1997), pp. 253–282. DOI: 10.1088/0266-5611/13/2/005 (cit. on p. C101).

[5] D. Colton and R. Kress. *Inverse Acoustic and Electromagnetic Scattering Theory*. 4th. Springer, 2019. DOI: 10.1007/978-3-030-30351-8 (cit. on pp. C100, C101, C102, C104, C110).

[6] M. Ganesh and S. C. Hawkins. "A far-field based T-matrix method for two dimensional obstacle scattering". In: *Proceedings of the 9th Biennial Engineering Mathematics and Applications Conference, EMAC-2009*. Ed. by P. Howlett, M. Nelson, and A. J. Roberts. Vol. 51. ANZIAM J. 2010, pp. C215–C230. DOI: 10.21914/anziamj.v51i0.2581 (cit. on p. C104).

[7] M. Ganesh and S. C. Hawkins. "A numerically stable T-matrix method for acoustic scattering by nonspherical particles with large aspect ratios and size parameters". In: *J. Acoust. Soc. Am.* 151 (2022), pp. 1978–1988. DOI: 10.1121/10.0009679 (cit. on p. C103).

[8] M. Ganesh and S. C. Hawkins. "Algorithm 975: TMATROM—A T-matrix reduced order model software". In: *ACM Trans. Math. Softw.* 44, 9 (2017), pp. 1–8. DOI: 10.1145/3054945 (cit. on pp. C102, C104, C110).

[9] M. Ganesh, S. C. Hawkins, and R. Hiptmair. "Convergence analysis with parameter estimates for a reduced basis acoustic scattering T-matrix method". In: *IMA J. Numer. Anal.* 32 (2012), pp. 1348–1374. DOI: 10.1093/imanum/drr041 (cit. on p. C103).

[10] M. Ganesh, S. C. Hawkins, A. M. Tartakovsky, and R. Tipireddy. "A stochastic domain decomposition and post-processing algorithm for epistemic uncertainty quantification". In: *Int. J. Uncertain. Quant.* 13 (2023), pp. 1–22. DOI: 10.1615/Int.J.UncertaintyQuantification.2023045687 (cit. on p. C105).

[11] S. C. Hawkins. "Algorithm 1009: MieSolver—An object-oriented Mie series software for wave scattering by cylinders". In: *ACM Trans. Math. Softw.* 46, 19 (2020), pp. 1–28. DOI: 10.1145/3381537 (cit. on p. C109).

[12] S. C. Hawkins. *Noisy far-field data*. Published online 12th August 2023. DOI: 10.5281/zenodo.8240111 (cit. on p. C109).

[13] T. Hohage. "On the numerical solution of a three-dimensional inverse medium scattering problem". In: *Inv. Prob.* 17 (2001), pp. 1743–1763. DOI: 10.1088/0266-5611/17/6/314 (cit. on p. C101).

[14] A. Kirsch and P. Monk. "An analysis of the coupling of finite-element and Nyström methods in acoustic scattering". In: *IMA J. Numer. Anal* 14 (1994), pp. 523–544. DOI: 10.1093/imanum/14.4.523 (cit. on p. C101).

[15] M. Löhndorf and J. M. Melenk. "On Thin Plate Spline Interpolation". In: *Spectral and High Order Methods for Partial Differential Equations ICOSAHOM 2016*. Ed. by M. Bittencourt, N. Dumont, and J. Hesthaven. Vol. 119. Lecture Notes in Computational Science and

Engineering. Springer, 2017, pp. 451–466. DOI: 10.1007/978-3-319-65870-4_32 (cit. on pp. C106, C109).

[16] T. D. Mast. "Empirical relationships between acoustic parameters in human soft tissues". In: *Acoust. Res. Lett. Online* 1 (2000), pp. 37–42. DOI: 10.1121/1.1336896 (cit. on p. C101).

[17] L. Stals. "Efficient Solution Techniques for a Finite Element Thin Plate Spline Formulation". In: *J. Sci. Comput.* 63 (2015), pp. 374–409. DOI: 10.1007/s10915-014-9898-x (cit. on p. C106).

[18] K. C. Tam. "Two-dimensional inverse Born approximation in ultrasonic flaw characterization". In: *J. Nondestruct. Eval.* 5 (1985), pp. 95–106. DOI: 10.1007/BF00566959 (cit. on p. C102).

[19] W. J. Wiscombe. "Improved Mie Scattering Algorithms". In: *Appl. Opt.* 19 (1980), pp. 1505–1509. DOI: 10.1364/AO.19.001505 (cit. on p. C106).

## Author addresses

1. **M. Ganesh**, Department of Applied Mathematics and Statistics, Colorado School of Mines, Golden Colorado 80410, USA.
2. **S. C. Hawkins**, School of Mathematical and Physical Sciences, Macquarie University, New South Wales 2109, AUSTRALIA.
3. **N. Kordzakhia**, School of Mathematical and Physical Sciences, Macquarie University, New South Wales 2109, AUSTRALIA.
4. **L. Stals**, Mathematical Sciences Institute, Australian National University, Canberra, AUSTRALIA.